JOURNAL OF MATERIALS SCIENCE 27 (1992) 3953–3962

High-temperature creep of the particle-hardened commercial Al–Li–Cu–Mg alloy 8090

C. K. L. DAVIES, S. POOLAY-MOOTIEN*, R. N. STEVENS, P. L. TETLOW
Department of Materials, Queen Mary and Westfield College, University of London, Mile End Road, London E1 4NS, UK

Creep of the particle-hardened commercial Al–Li 8090 alloy has been studied at temperatures of 425 and 445 K. The measured stress sensitivity of the minimum creep rates changes abruptly at a given applied stress with stress exponents being around 4–6 at low stresses and 30–40 at high stresses. Creep activation enthalpies were determined by both temperature cycling and by comparing creep rates at two temperatures at a given applied stress, the results from both gave the same unrealistically high values. The internal stresses, σ_i, developed during creep were determined using the strain-transient dip test. These increased linearly with the applied stress, σ_a, at low stresses and were effectively constant at high stresses. The minimum creep rate was found to be a simple function of the effective stress, $\sigma_a - \sigma_i$, with a stress exponent of between 5 and 6, at all applied stresses. The dislocation and precipitate structure of the alloy was examined before and after creep using thin-film electron microscopy. The initial structure consisted of pancake grains with a well-developed $\{1\,1\,0\}\langle 1\,1\,2\rangle$ type texture. The grains contained well-developed sub-cells and δ' and S precipitates. The structure developed during creep consisted of dislocation pairs, single dislocations and dislocations loops. There was evidence to suggest that slip took place on both $\{1\,0\,0\}$ and $\{1\,1\,1\}$ planes. The dislocation loops were most likely to have been Orowan in character and around the rod-like S precipitate, with the coherent δ' precipitate being sheared by pairs of dislocations. The measured internal stresses result from inhomogeneity of plastic deformation. These stresses increase continuously with applied stress up to the observed macroscopic yield stress, and then become constant. The internal stresses are likely to have arisen from the Orowan loops around S and the behaviour of sub-grain boundaries. The increases in internal stress may have resulted from an increased loop density with increasing applied stress. This rate of increase is likely to slow down if S particles are sheared or fractured at high applied stresses.

1. Introduction

Creep in particle-hardened alloys has been studied most extensively for systems in which nickel is the major element [1–10]. These alloys are either strengthened with γ' (Ni_3Al), an ordered $L1_2$ superlattice structure, or by undeformable oxide particles. The creep properties of these alloys are characterized, at least at high stresses, by a very high stress dependence of the minimum creep rate, the exponent n in the relation between creep rate, $\dot{\varepsilon}$, and applied stress, σ_a, $\dot{\varepsilon} = A\sigma_a^n$, where A is a constant, being in the range 10–40. These stress dependences have been explained by the fact that creep is driven by the effective stress, $\sigma_a - \sigma_o$, rather than the applied stress, σ_a.

Recently it has been suggested that σ_o is an internal stress [9, 10] as defined by Gibeling and Nix [11] which can be determined, at least approximately, by the strain-transient dip test [11]. It has been demonstrated, at least for Nimonic 91, that major contributors to this internal stress were Orowan loops around γ' particles [9, 10].

Dilute, single-phase, Al–Li alloys behave in the main as Class II alloys with stress exponents of 4–5, and with creep being controlled by dislocation climb [12–14]. There are suggestions, however, of Class I, viscous glide behaviour at certain stresses and temperatures [13–15]. Higher concentration Al–Li alloys are strengthened by spherical metastable δ' precipitates (Al_3Li), which are isomophorous with γ' in nickel alloys and have the same cube–cube matrix/precipitate orientation relationship. The δ' precipitates harden the alloys, because particles are cut by dislocations producing anti-phase boundaries at small particle spacings and dislocations form Orowan loops around the particles at larger particle spacings [15–18]. Orowan loops have been observed in Al–Li alloys at temperatures as high as 493 K, some of which have a surprising long-term stability [18]. The addition of copper and magnesium to the alloys results in the precipitation of S (Al_2CuMg) and T_1 (Al_2CuLi) phases which are not easily sheared by matrix dislocations [17, 19, 20]. The presence of the T_1 phase, at least,

* Research visitor from University of Aix-Marseille II, France.

0022–2461

seems to lower the particle size at which the transition from looping to cutting occurs. Harris *et al.* [21] noted a pronounced effect of the S precipitates on the creep rate when comparing creep of an Al–Li–Mg–Zr alloy with that of an Al–Li–Mg–Cu–Zr alloy (8090). The former alloy contained primarily δ′ precipitate, while the latter contained additionally S precipitated predominantly on sub-grain boundaries. The stress exponent of the creep rate for the alloy containing S was about 28 while for the alloy containing only δ′ it was around 8. Hayashi and Oikawa [22] confirmed the high stress dependence for the 8090 alloy during creep at high temperatures (500–650 K) and relatively low stresses (10–100 MPa). They reported stress exponents of 5–10 at low stresses and 13–32 at high stresses which are characteristic of particle-hardened alloys in general. It was suggested that creep was controlled by an initial effective stress, $\sigma_a - \sigma_{th}^o$, with a stress exponent of 3.6. The exact nature of the precipitates present and their distribution was unclear, as are the meaning and method of determination of the initial threshold stress σ_{th}^o.

The present work was a study of the creep of a carefully characterized 8090 alloy, containing primarily δ′ and S precipitates. The internal stress was measured using the strain-transient dip test [9–11]. Thin-film electron microscopy was used to study dislocation structures and slip systems operating during creep and in particular to study the role of δ′ and S in determining the internal stress and the creep rate.

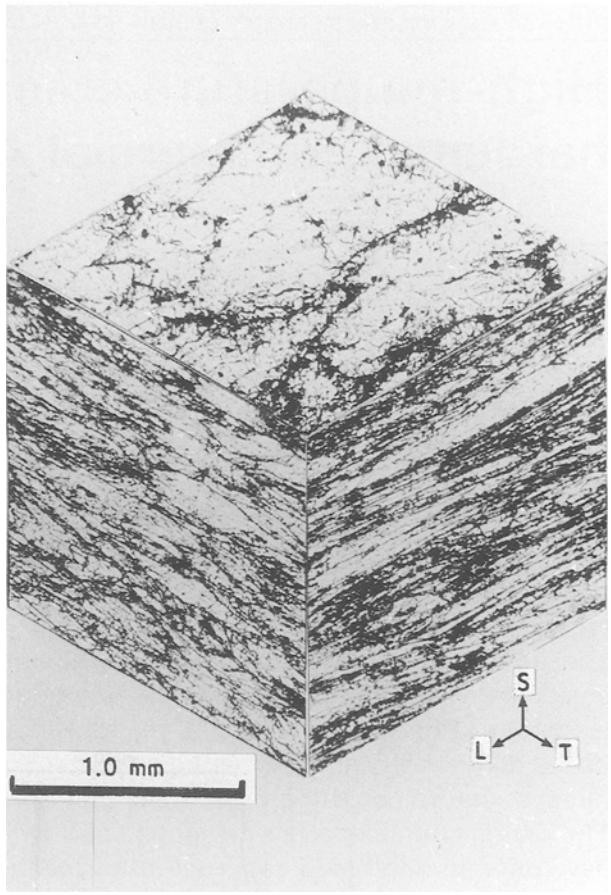

Figure 1 Grain structure of 8090 alloy shown in three orthogonal planes.

2. Experimental procedure

The 8090 alloy was supplied by Alcan via RAE Farnborough in the form of a 60 mm thick plate of overall composition: Li 2.3, Cu 1.2, Mg 0.67, Zr 0.13, balance aluminium (all in mass %). The plate had been solution treated at 803 K for 30 min, water quenched and given a 2.5% stretch prior to ageing at 463 K for 16 h. The plate had anisotropic mechanical properties and an anisotropy of structure. The grain structure (Fig. 1) consisted of pancake grains of mean dimensions 1.0 mm × 0.5 mm × 0.05 mm in the directions L (longitudinal), T (transverse), S (short transverse). Cylindrical creep specimens with threaded ends, 25.4 mm gauge length and of diameter 4.50 mm were machined from the plate with the axis of the specimens being in the L direction. The mechanical properties of the material varied through the thickness of the plate. Hence all creep specimens were machined from bars cut from the plate so that their centre lines lay at a depth below the surface of one-quarter of the plate thickness. Such specimens gave reproducible room-temperature mechanical properties.

Constant stress tensile creep tests were performed in air, with loading via an Andrade Chalmers cam [23, 24] over the stress range 200–450 MPa at temperatures of 425 and 445 K. The specimens were heated via a three-zone furnace and the temperature was controlled to ± 1.0 K over the specimen gauge length using three thermocouples and a three-term temperature controller. Strain was measured using linear variable capacitance transducers capable of detecting displacements of 10^{-8} m with an extensometer system resolving strains to $\pm 2 \times 10^{-5}$. Strain/time data were captured via a BBC micro-computer [25]. Strain-transient dip tests were performed as described previously [9, 10].

Lattice parameters were determined using a Debye–Scherrer X-ray camera with Straumanis film mounting. Pole figures were determined using a computerized diffractometer at RAE, Farnborough.

For transmission electron microscopy (TEM) thin foils were prepared from slices 0.35 mm thick cut from the creep specimen gauge length and spark eroded to 3 mm diameter discs and polished to a thickness of 0.25 mm on 1000 grade SiC paper. The discs were electropolished using a jet polishing apparatus [24] and an electrolyte of 25% nitric acid in methanol at − 15 °C at 8–10 V and 35–40 mA. The resulting thin foils were examined in a Jeol 100CX transmission electron microscopy using bright-field (BF), two-beam bright-field (TBBF), centred dark-field (CDF), and weak-beam imaging modes. Film thicknesses were measured using a convergent-beam technique [24, 26].

3. Results and discussion

3.1. Structure of alloy 8090

The alloy is anisotropic with a pancake grain structure as shown in Fig. 1. The material exhibits a $\{1\,1\,0\}\langle 1\,1\,2\rangle$ type texture with the rolling direction, the tensile axis of the creep specimens, approximating

to ⟨1 1 2⟩. This texture becomes more developed during creep (Fig. 2). Within the grains is a well developed sub-grain structure (Fig. 3) with approximate mean dimensions of 25 μm × 20 μm × 10 μm (L–T–S). The dimensions of this substructure do not appear to change on ageing at temperatures of 423–463 K or during creep tests at 425 and 445 K, of duration up to 50 days.

The initial structure contains spherical δ′ particles of mean diameter 23 nm with a size distribution of between 0.25 and 2.0 times this value. This mean value drops to 21.5 nm during ageing, prior to the start of a creep test. The δ′ particles coarsen during ageing with mean particle diameters increasing as $t^{1/3}$, reaching diameters of 32 and 38 nm after 1000 h at 425 and 445 K, respectively, with evidence of particle coalescence [27] (Fig. 4). The particle-size distribution becomes more skewed with increasing ageing time. The average δ′ particle diameters measured after creep tests correspond to those determined after similar ageing times in unstrained specimens. The volume fraction of δ′ increases with ageing time from an initial value of 5%, to 8% after 150 h at 445 K and 212 h at 425 K. This is accompanied by a small but continuous increase in matrix lattice parameter. A similar volume fraction increase is observed in creep-tested specimens. The volume fractions were determined by measuring foil thicknesses using a convergent beam technique and by counting the numbers and measuring the diameters of δ′ particles. Allowance was made for particles cut by the foil surface (as observed in the SEM) which reduced the volume fractions from apparent values of up to 10% after ageing [24]. This effect of particle sectioning by the foil surface can be used to explain, in a large part, the apparent skewing of particle size distributions at long ageing times [24]. This continuous increase in δ′ volume fraction at relatively long ageing times has been observed previously in both binary and quaternary Al–Li alloys [28–30], although in these cases the effect of foil surface sectioning was not allowed for. The reason for this apparent increase is not clear. The simplest explanation would be a movement of the δ′ solvus as a function of time as a result of time-dependent partitioning of copper and magnesium to or from δ′

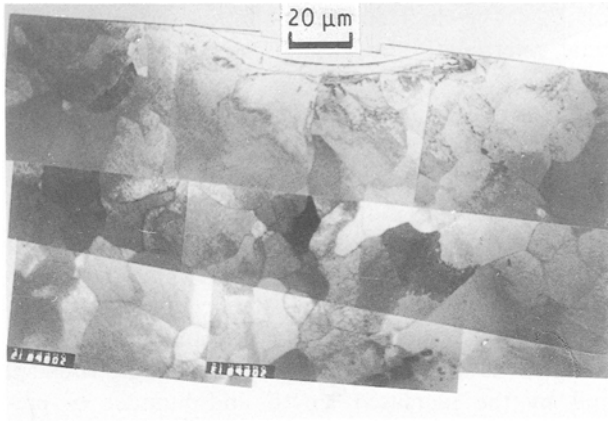

Figure 3 Transmission electron micrograph collage showing 8090 subgrain structure; L–T plane.

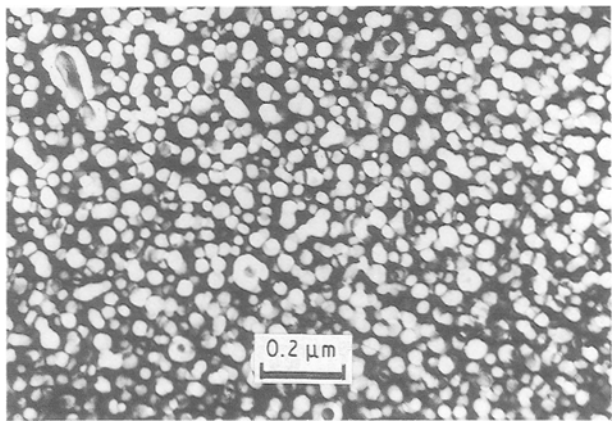

Figure 4 Transmission electron (CDF) micrograph **B** = ⟨0 0 1⟩ using {1 0 0} δ′ spot. 300 MPa/425 K test. Precipitate necklaces and coalescence.

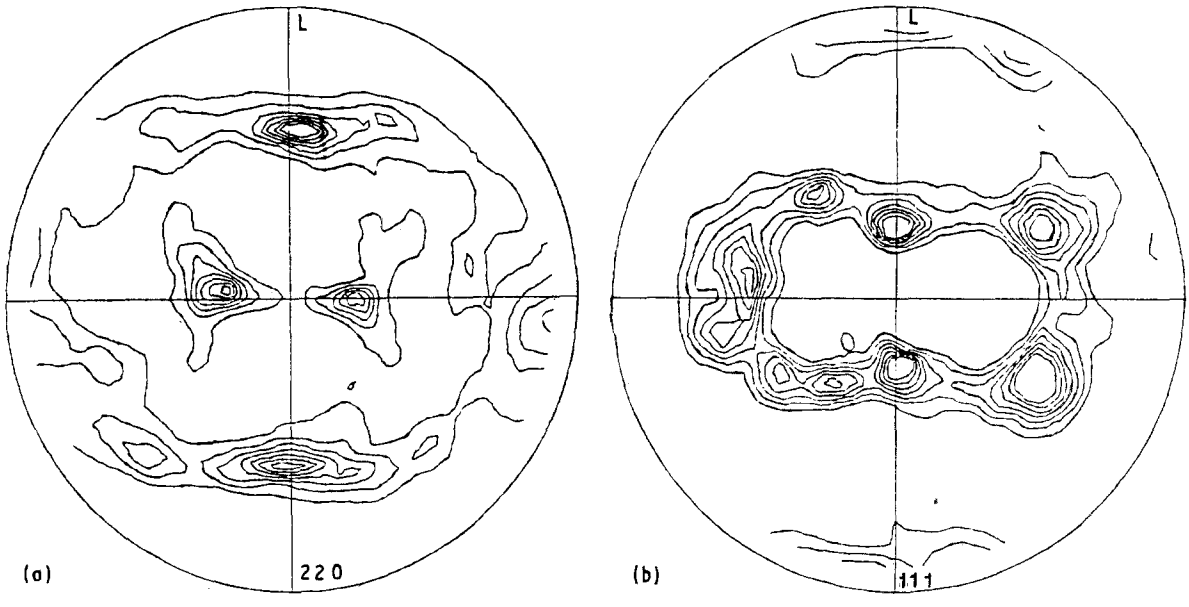

Figure 2 Texture pole figures for 8090 alloy after creep: (a) {2 2 0}, (b) {1 1 1}.

[31, 32]. The change in matrix lattice parameter with time, referred to above, lends some support to this argument.

The initial structure also contained needles of the orthorhombic S precipitate lying along ⟨0 0 1⟩ matrix directions, within the sub-grains and at sub-grain boundaries. The initial precipitates were approximately 5 nm diameter and of length 200 nm with a volume fraction of approximately 0.1%. Ageing for up to 39 days at 443 K caused the volume fraction to increase to 0.5% as evinced by the pronounced brightening of the S spots in the diffraction pattern (Fig. 5a) and by the increased length and number of precipitates observed in bright-field (Fig. 5b). S precipitates were also observed to increase in length and number during creep tests but seem to be limited to a length of 300 nm even after very long-term tests.

The T_1 phase could not be detected in the initial material. After long-term creep tests, apparent images of the T_1 phase appeared to a limited extent in the appropriate two-beam bright-field condition, although T_1 diffraction spots were barely discernible, if not invisible.

3.2. Mechanical test results

The creep curves obtained at both 445 and 425 K were of normal shape with the strain rate continuously decreasing in primary, constant in secondary and accelerating in tertiary creep until fracture (Fig. 6). The initial strain upon loading is largely elastic until about 400 MPa, above which significant plastic deformation takes place (Fig. 7). The elastic strain follows that predicted by the modulus measurements (Fig. 8). Both the primary creep strain (Fig. 9) and the secondary creep strain (Fig. 10) are small at low stresses but increase continuously at high stresses. The measured minimum creep rates are shown as a function of applied creep stress in Fig. 11. The stress sensitivity of the creep rate changes abruptly at 330 MPa at 425 K and at approximately 300 MPa at 445 K, the stress exponents being around 4.5 below the break and 35 above the break at 425 K and much more approximately 7.5 and 44 at 445 K. Approximate values of the

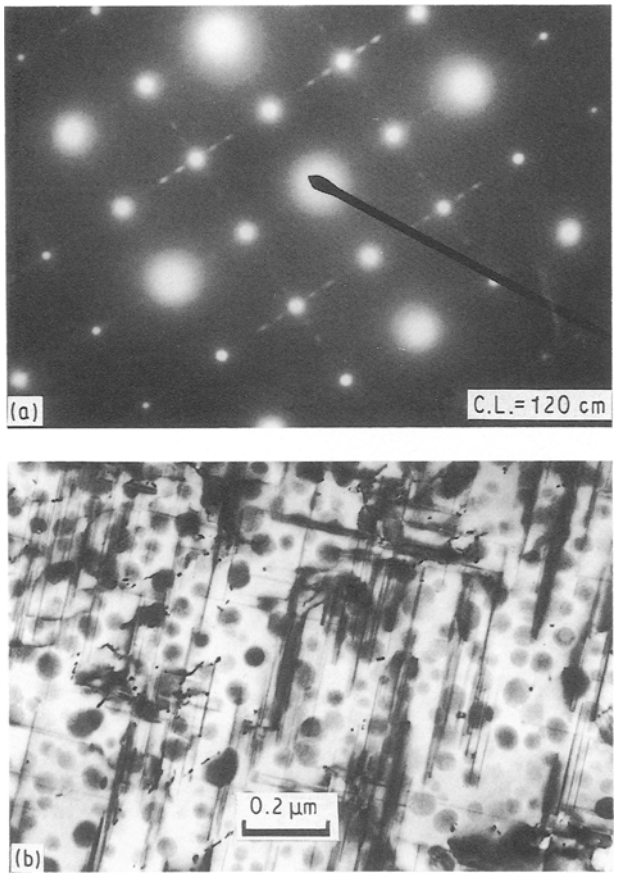

Figure 5 (a) Selected-area diffraction pattern using $\mathbf{B} = \langle 0\,0\,1 \rangle$ showing δ′ and matrix spots plus S streaks. Material aged for 39 days at 443 K. (b) Transmission electron (BF) micrograph $\mathbf{B} = \langle 0\,0\,1 \rangle$ of material in (a).

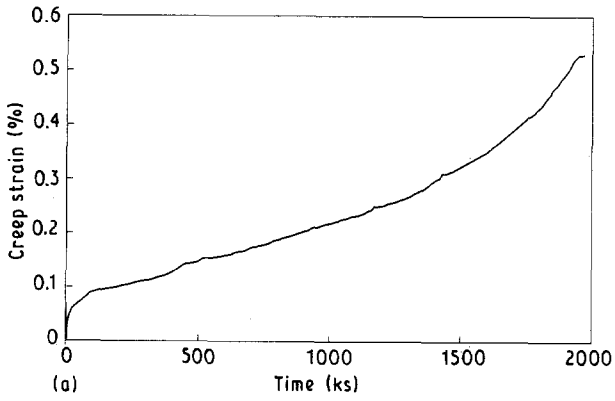

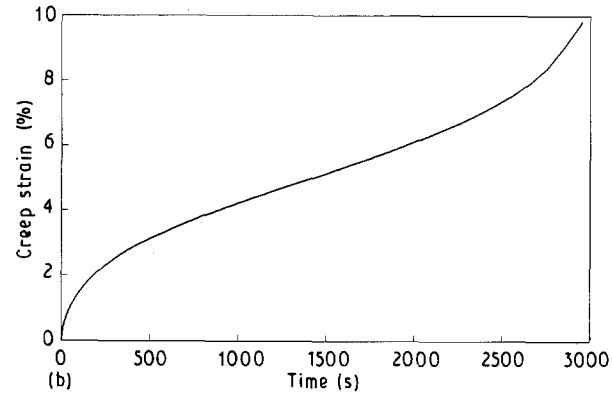

Figure 6 Creep curves for (a) a 300 MPa test at 425 K, (b) a 420 MPa test at 425 K.

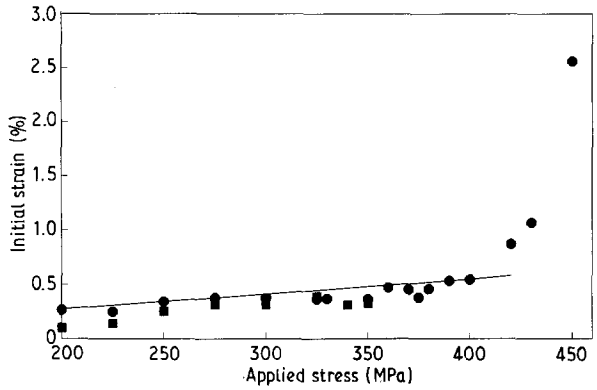

Figure 7 Initial strain on loading, versus applied stress for (●) 425 and (■) 445 K creep tests; (——) modulus line (73 GPa) for 425 K tests.

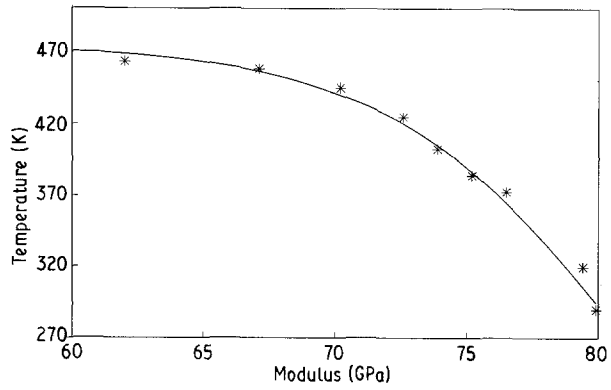

Figure 8 Tensile modulus versus temperature for the 8090 alloy.

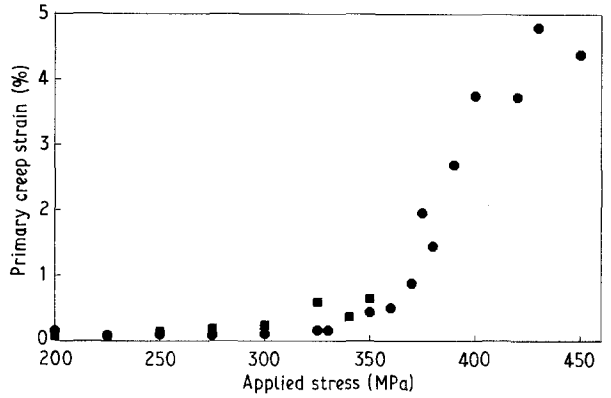

Figure 9 Primary creep strain versus applied stress for (●) 425 and (■) 445 K creep tests.

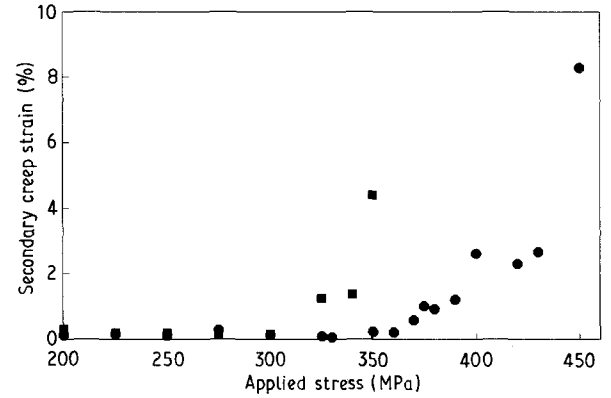

Figure 10 Secondary creep strain versus applied stress for (●) 425 and (■) 445 K creep tests.

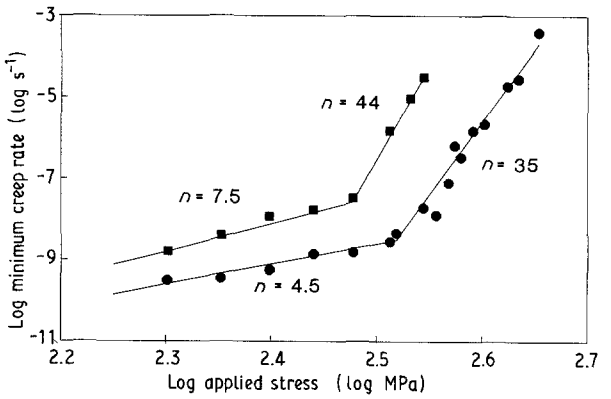

Figure 11 Minimum creep rate versus applied stress for (●) 425 and (■) 445 K creep tests.

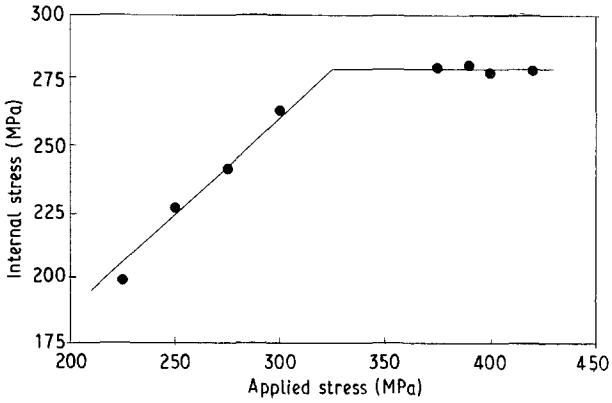

Figure 12 Internal stress versus applied stress from strain-transient dip tests at (●) 425 K.

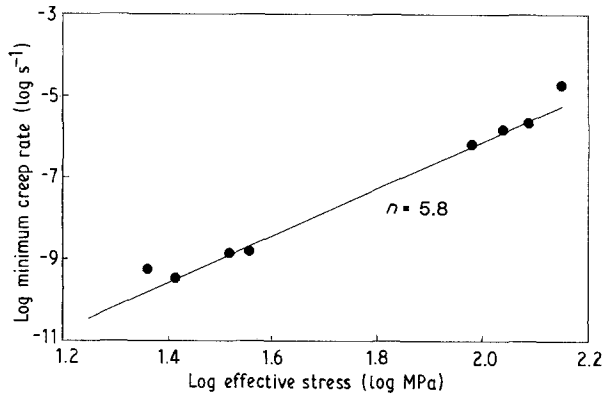

Figure 13 Minimum creep rate versus effective stress for (●) 425 K creep tests.

internal stress were determined at 425 K using the strain-transient dip test and are shown in Fig. 12 as a function of applied stress. The internal stress increases linearly with applied stress below an applied stress of 330 MPa and becomes constant at high applied stresses. The creep rate is shown as a function of the effective stress, $\sigma_a - \sigma_i$, in Fig. 13 where the data are represented by a single line with a stress exponent of between 5 and 6.

Activation enthalpies were measured by both temperature cycling and by comparing the creep rates at the two temperatures at a given applied stress. The results gave unrealistically high values of approximately 580 kJ mol^{-1} at high stresses and 240 kJ mol^{-1} at low stresses.

Fracture occurs as a result of cracks growing either along the major grain boundaries nearly parallel to the stress axis or at 45° to this direction, the former being predominant at the highest stresses. Pronounced slip bands were seen in fractured specimens, tested just above the high-temperature yield stress but these were absent in the highest stress tests. The time to fracture increased as the minimum creep rate decreased (Fig. 14).

3.3. Dislocation structures developed during creep

Thin foils were examined from creep specimens stopped in secondary creep and from fractured specimens.

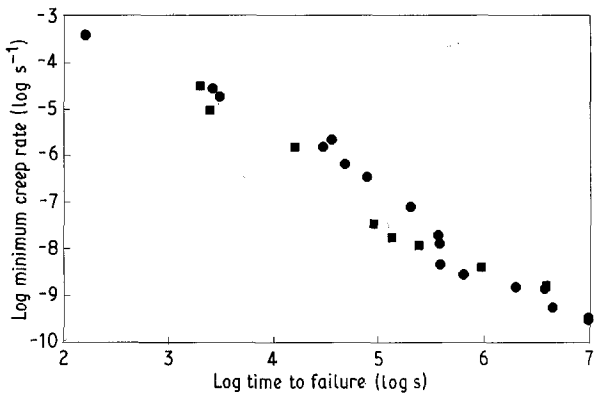

Figure 14 Minimum creep rate versus time to failure for (●) 425 and (■) 445 K creep tests.

The results are not unambiguous, because it is often difficult to distinguish between the structures developed during the initial extension, during primary and secondary creep and those developed during the rapid strain prior to fracture. In specimens stopped during secondary creep, at all but the highest stresses, bowing single dislocations are seen often accompanied by dislocation loops (Fig. 15a) and or pairs of dislocations (Fig. 15b). In most cases slip seems to be planar and only at the highest stresses are dislocation tangles developed in some sub-grains (Fig. 15c). The picture in fractured specimens is similar, consisting of single dislocations, bowing dislocations and dislocation pairs (Fig. 16a–c). Two surprising features are observed, firstly in all but the very shortest creep tests the dislocations are decorated by a precipitate, and secondly by far the majority of single dislocations lie close to $\langle 1\,1\,0\rangle$ and the majority of pairs lie close to $\langle 1\,0\,0\rangle$.

If specimens are dark-field imaged using known S spots in the $(0\,0\,1)_m$ matrix diffraction pattern, both the dislocation precipitate and the S precipitate in the matrix appear bright. However, the decorating precipitate does not lie on the dislocations in one of the two normally observed S matrix orientations (i.e. $[1\,0\,0]_m$ and $[0\,1\,0]_m$ in an $[0\,0\,1]_m$ bright-field image) but at about 25° to one of these corresponding to a $\langle 2\,1\,0\rangle_m$ orientation. It produces an extraneous spot in the $(0\,0\,1)_m$ diffraction pattern (rotated about 25° away from $\boldsymbol{g} = (0\,1\,0)_m$ and with a radial displacement corresponding to an interplanar spacing of 0.46 nm) which when used to produce a dark-field image only shows the precipitate on the dislocations to be bright. The S precipitate is known to form on $\{2\,1\,0\}$ matrix planes as laths orientated in a $\langle 1\,0\,0\rangle$ matrix direction [33]. Specifically, in an $(0\,0\,1)_m$ bright-field image, precipitate laths growing on a $(1\,2\,0)_m$ plane in an $[0\,0\,1]_m$ direction would be viewed end on down their $[1\,0\,0]_s$ axis direction (Fig. 17). The $[1\,2\,0]_m$ direction would thus correspond to the $[0\,1\,0]_s$ direction. This should then produce an $(0\,2\,0)_s$ spot in the $(0\,0\,1)_m$ pattern having a rotation of 26.5° about the beam direction and a displacement corresponding to an interplanar spacing of 0.463 nm. There would normally not be sufficient S in this orientation to produce the spot in the $(0\,0\,1)_m$ pattern but the high density of S on the dislocations makes it visible.

The fact that the dislocations are decorated with S is hence reasonably certain, the question remains, however, as to whether this decoration process occurs during creep or when specimens are cooled to room temperature. Dislocations in solution-treated specimens are free of precipitate even after ageing at room temperature for 1 year, as are dislocations in specimens crept at very high stresses for short times. It seems most probable then that the precipitation takes place at the creep temperature. This would almost

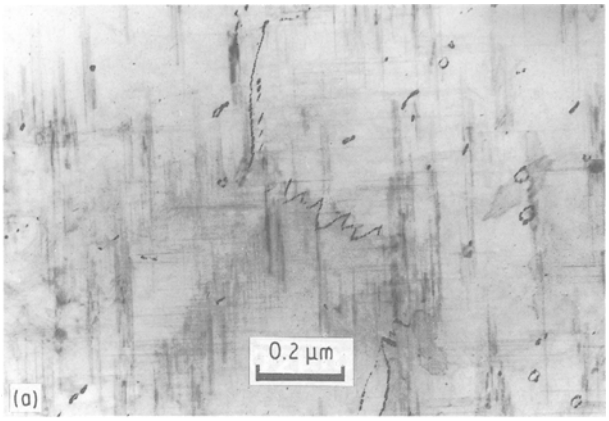

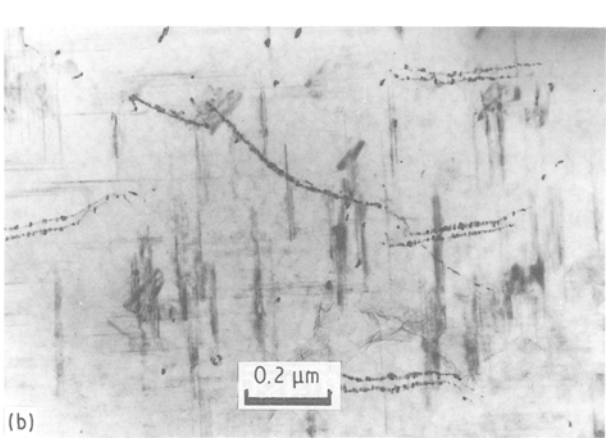

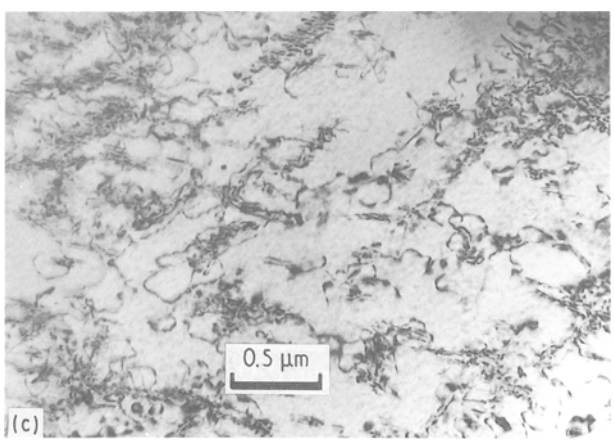

Figure 15 (a) Transmission electron (TBBF) micrograph **B** close to $\langle 0\,0\,1\rangle$ using $\{2\,0\,0\}$. 430 MPa/425 K creep test stopped in secondary creep showing looping and bowing dislocations. (b) As (a) showing decorated paired dislocations. (c) Transmission electron (TBBF) micrograph **B** close to $\langle 1\,1\,0\rangle$ using $\{1\,1\,1\}$. 400 MPa/425 K creep test stopped in secondary creep showing dislocation tangles.

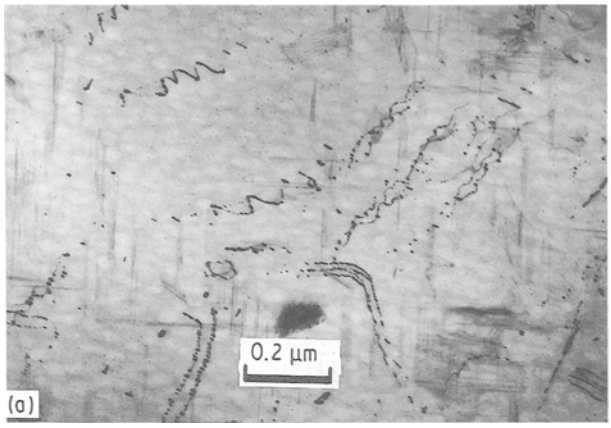

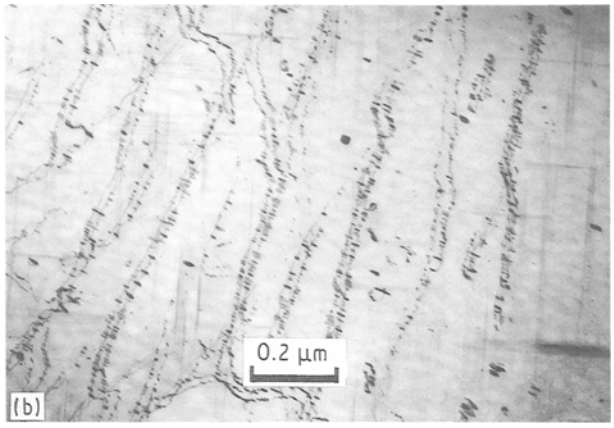

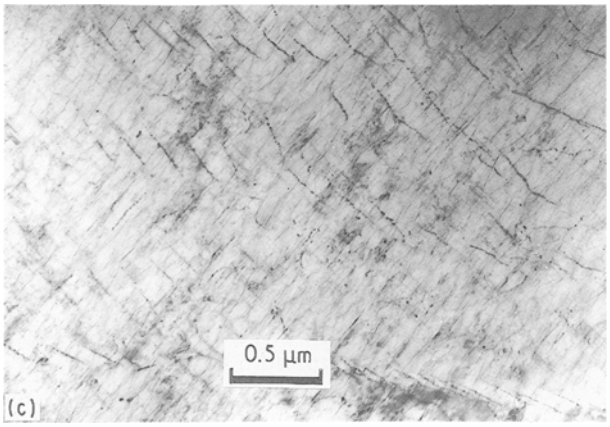

Figure 16 Transmission electron (TBBF) micrograph **B** close to ⟨0 0 1⟩ using {2 0 0}. 300 MPa/425 K fractured creep test showing paired and bowing dislocations. (b) As (a) showing long paired decorated dislocations. (c) Transmission electron (TBBF) micrograph **B** close to ⟨0 0 1⟩ using {2 0 0}. 350 MPa/445 K fractured creep test showing array of decorated dislocations.

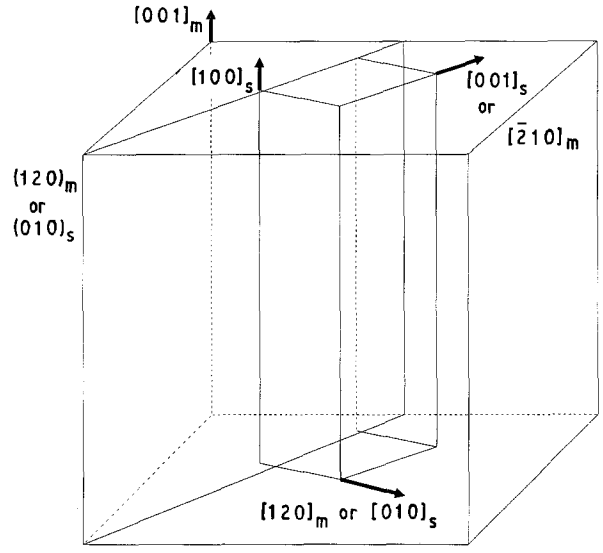

Figure 17 The orientation relationship between the S(Al_2MgCu) precipitate, producing the extraneous spot in an {0 0 1} diffraction pattern, and the matrix.

certainly pin the dislocations, if they are not already pinned. At high stresses it is possible that either dislocations break free of the precipitates or their velocity is such that precipitation does not occur. Precipitation of S takes place during creep at subboundaries and in the matrix and hence would be expected to form on any relatively immobile dislocations.

As stated above, when viewing {0 0 1} transmission electron micrographs of crept specimens the majority of paired dislocations are orientated close to ⟨1 0 0⟩ directions (Figs 15b and 16b) while most of the single dislocations are orientated close to ⟨1 1 0⟩ (Figs 15a and 16a). In both cases long lengths of dislocation line can be observed. The normal deformation mode for fcc materials is {1 1 1}⟨1 1 0⟩ and if slip were occurring in, say, (1 1 1) then long lengths of single dislocation line could be attributed to dislocations lying along the [$\bar{1}$ 1 0] direction, as this vector for the (1 1 1) plane is normal to the {0 0 1} beam or viewing direction (Fig. 18a). However, because of the orientation of the dislocation pairs, if these were lying on the (1 1 1) plane, their line length would be limited by the projection of this plane within the foil thickness (Fig. 18b) and thus it is difficult to explain these long lengths (Fig. 16b) by normal {1 1 1}⟨1 1 0⟩ slip. This raises the interesting possibility that the pairs are not lying on {1 1 1} planes but on or close to {1 0 0} planes.

The {1 0 0}⟨1 1 0⟩ slip system is known to operate in [1 1 2] aluminium single crystals during creep tests at temperatures as low as 453 K and to become increasingly easy as the temperature is raised [34, 35]. It is also known to occur in materials with an LI_2 structure i.e. $\gamma'(Ni_3Al)$, at temperatures as low as 0.4–0.6 of the absolute melting temperature [36], as slip on (0 1 0) planes results in no first nearest neighbour atomic violations of structure yielding a minimum anti-phase boundary energy [37]. Furthermore, the orientation texture in the present material is such that a majority of crystals will have ⟨1 1 2⟩ closely aligned to the tensile axis and hence the Schmid factors for {1 0 0}⟨1 1 0⟩ slip are almost always higher than those for {1 1 1}⟨1 1 0⟩ slip.

From the above it can be seen that there is evidence to suggest that both {1 1 1}⟨1 1 0⟩ and {1 0 0}⟨1 1 0⟩ slip operate during creep in 8090 at 425–445 K. This would explain the dislocation geometries seen in that most of the pairs lie on {1 0 0} planes, e.g. Fig. 16b, and are of 45° mixed edge and screw character, although in rare cases pairs on {1 1 1} can be found,

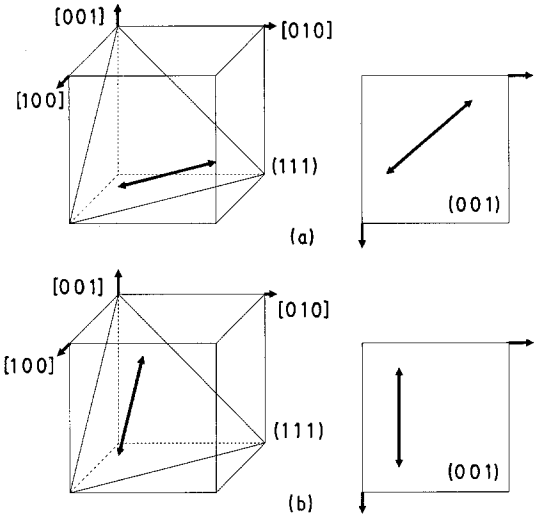

Figure 18 The projection of (a) the [− 1 0 1] direction and (b) the [− 1 1 0] direction in the (1 1 1) plane on to the (0 0 1) plane.

which could be either screw in character or 60° mixed. Most of the single dislocations are, however, operating on {1 1 1} planes and when long, are predominantly of screw or 60° mixed character and when short are either of edge or 30° mixed character. Furthermore some of the apparently "bowing" dislocations (Figs 15b, 16a) could consist of screw dislocations with segments on both {1 1 1} and {1 0 0} planes [35, 38] The above speculation must be treated with some caution, especially as the effect of S precipitate on the dislocations may well affect their orientations.

3.4. Creep and the internal stress

The creep behaviour of 8090 exhibits similarities with that of nickel-base alloys strengthened with γ′ or oxide particle dispersions [1–10]. The applied stress sensitivity of the creep rate is very high at high stresses decreasing to more normal values at low stresses (Fig. 11). The internal stress increases linearly with applied stress at low stresses and is approximately constant at high stresses (Fig. 12) as for Nimonic 91 [9, 10]. Furthermore, the creep rate is seen to be a simple function of the effective stress (Fig. 13) as found for Nimonic 91 and other nickel-base alloys. In common with other particle-hardened alloys, anomalously high creep activation enthalpies are found particularly at high stresses. This may, in part, arise from the use of creep rates at constant values of applied stress to determine the activation enthalpy. It is arguable that creep rates at constant values of effective stress should be used.

The internal stress arises as a result of the inherent inhomogeneity of plastic deformation in two-phase alloys. In the case of Nimonic 91 [9, 10], it was possible to show that the internal stress was primarily due to the presence of Orowan loops around γ′ particles at low stresses, which increased in number with increasing creep stress, resulting in an approximately linear increase in internal stress. At high stresses, partial or complete shearing of γ′ particles, held the internal stress approximately constant.

In the present case the situation is much more complex. The 8090 alloy has a well developed substructure containing both spherical δ′ particles and rods of S.

Dislocation loops are observed which may be Orowan in character (Fig. 19), as well as dislocation pairs suggesting that δ′ particles are sheared. The transition from cutting to looping occurs at a δ′ particle size of around 30 nm in the Al–Li 3% binary alloy with a 25% volume fraction of δ′ [17] but is reduced considerably in the presence of the T phase [17]. Orowan loops around δ′ have been observed in binary alloys with surprising long-term stability at temperatures as high as 493 K [18]. It is presumed, here, that these are stable due to partial penetration of the δ′ particles and cannot climb easily within the particles because of the high energy of the resulting faults as for Nimonic 91 [9, 10]. The stress at which looping of δ′ would occur for the current particle size of 23–38 nm and volume fractions of 5%–8% is by no means clear, as under creep conditions looping often occurs well below the theoretical stress determined using the average particle spacing, as dislocations seek out the largest particle spacing [9, 10, 25]. In the present case it is clearly not possible to eliminate the possibility that some of the observed loops are around δ′ particles.

The S and T_1 phases will not be easily sheared by matrix dislocations and are known to have a significant effect on maintaining mechanical strength up to high temperatures [21, 39]. Xiaoxin and Martin [40] found the work-hardening rate at elevated temperatures to be a maximum for alloys containing the largest volume fraction and size of the S precipitate. Furthermore, it has been demonstrated that the presence of S significantly decreases observed creep rates and dramatically increases the stress dependence of the creep rate [21]. It is likely, then, that the S rods are Orowan looped. It must be remembered that the S structure develops with time during creep, offering most resistance to dislocation motion at the lowest stress, although at these low stresses dislocation motion is slow and minimal, enabling them to bypass some S particles. At the very highest stresses, S may be sheared by {1 0 0} matrix dislocations, by twinning or

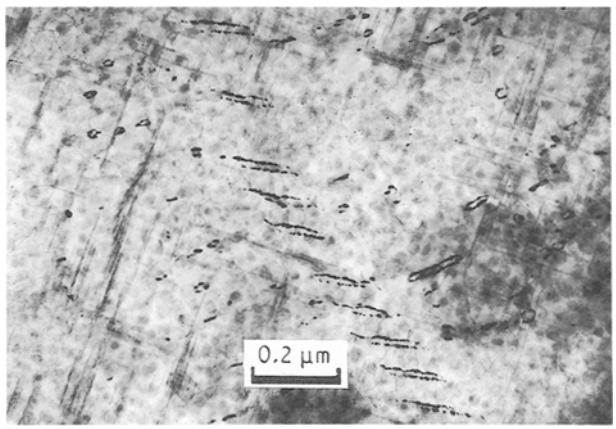

Figure 19 Transmission electron (TBBF) micrograph **B** close to ⟨0 0 1⟩ using {2 0 0}. 400 MPa/425 K fractured creep test showing loops and an assemblage of paired dislocations.

fracture [41]. It is most likely, then, that the loops observed are Orowan in nature around S rods which are stable against climb due to the long climb distances involved (200–300 nm).

Apart from the presence of Orowan loops, the sub-grain cell walls themselves may contribute to the internal stress [42] as well as causing inhomogeneities of deformation from one cell to another.

The present results show that the measured internal stress increases with applied stress (Fig. 12) up to the point at which significant plastic deformation takes place during the initial extension, (Fig. 7), during primary creep (Fig. 9) and during secondary creep (Fig. 10). It may well be that this increase in internal stress results from an increasing density of Orowan loops, mostly around S, and increased bowing of sub-grain walls. Above this stress, deformation becomes more extensive but more homogeneous with slip bands transversing cell boundaries, orientated consistent with $\{1\,1\,1\}$ or $\{1\,0\,0\}$ slip. At even higher stresses, dislocation networks develop and S particles may be sheared, resulting in relatively homogeneous deformation coinciding with a relatively constant internal stress.

While this very qualitative description may illustrate the behaviour of the internal stress as a function of applied stress, explanations of creep process are much less certain. The creep process above and below the break may be similar, differing only as a result of the change in internal stress. Alternatively, creep may occur at low stresses by single dislocations or pairs wiggling their way across slip planes, seeking out the easiest paths via local climb, under the action of the effective stress. However, at the highest stresses creep may be recovery controlled by dislocation motion in a network, the dimensions of which are related to the hard particle spacing.

4. Conclusions

Creep in this particle-hardened commercial Al–Li, 8090, alloy shows great similarity to the behaviour observed in nickel-based alloys hardened with γ'. The stress dependence of the creep rate is exceptionally high ($n = 35$–45) and unrealistically high values of the creep activation enthalpy are determined. This high stress dependence can be explained, if creep is driven by the effective stress, $\sigma_a - \sigma_i$, rather than by the applied stress, σ_a. The applied stress dependence of the internal stress, σ_i, as measured by the strain-transient dip test, also mirrors that observed for nickel-based alloys [9, 10], σ_i increasing linearly at low creep stresses but becoming approximately constant at high stresses. The exact origin of the internal stress is uncertain. It is clear, however, that it is the inhomogeneity of plastic deformation at low stresses which is the general source and that the looping around rods of S precipitate must make a contribution. When large-scale near-homogeneous plastic deformation takes place, at high stresses, the internal stress ceases to rise. The detailed role of δ', S and the sub-boundaries in this process could only be studied in any fundamental way by testing Al–Li–X alloys in which both the precipitate structure and dislocation microstructure could be varied significantly, i.e. δ' with no S, S or T with no δ', and δ' of such a size that it is sheared or looped, etc. One other interesting possibility, suggested by this work, is that some $\{1\,0\,0\}\langle 1\,1\,0\rangle$ slip may occur during creep. Whether this is a general phenomenon in Al–Li alloys or is peculiar to the well-developed texture in this alloy needs to be investigated further, particularly in higher volume fraction δ' alloys at higher temperatures.

Acknowledgements

The authors thank Dr D. S. McDarmaid, R. A. E. Farnborough, and Alcan International for supplying the alloy.

References

1. K. R. WILLIAMS and B. WILSHIRE, *Met. Sci. J.* **7** (1973) 176.
2. W. J. EVANS and G. F. HARRISON, *ibid.* **10** (1976) 307.
3. J. P. DENNISON, P. D. HOLMES and B. WILSHIRE, *Mater. Sci. Engng* **33** (1978) 35.
4. S. PUROSHOTHAMAN and J. K. TIEN, *Acta Metall.* **26** (1978) 519.
5. H. BURT, J. P. DENNISON and B. WILSHIRE, *Met. Sci. J.* **13** (1979) 295.
6. M. McLEAN, *Proc. Roy. Soc.* **A373** (1980) 93.
7. R. A. STEVENS and P. E. J. FLEWITT, *Acta Metall.* **29** (1981) 867.
8. W. J. EVANS and G. F. HARRISON, *Met. Sci. J.* **13** (1979) 641.
9. C. K. L. DAVIES, A. G. OLDER and R. N. STEVENS, in "Proceedings of 4th International Conference on Creep and Fracture of Engineering Materials and Structures", Swansea, UK, April 1990, edited by R. W. Evans and B. Wilshire (Institute of Metals, London) pp. 97–107.
10. *Idem, J. Mater. Sci.*
11. J. C. GIBELING and W. D. NIX, *Mat. Sci. Engng* **45** (1980) 123.
12. D. O. NORTHWOOD and I. O. SMITH, *Phys. Status Solidi* **88A** (1985) 181.
13. A. R. ALI, M. A. FAHIM and F. M. MANSY, *J. Mater. Sci. Lett.* **8** (1989) 841.
14. KYUNG-TAE PARK, ENRIQUE J. LAVERNIA and FARGHALLI A. MOHAMED *Acta. Metall. Mater.* **38** (1990) 1873.
15. Y. MIURA, A. MATSUI, M. FURUKAWA, M. NEMOTO, in "3rd Al–Li Conference", Oxford, 1985, edited by C. Baker, P. J. Gregson, S. J. Harris and C. J. Peel (Institute of Metals, London, 1986) pp. 427–434.
16. J. M. FRAGOMENI, B. M. HILLBERRY and G. H. SANDERS, in "5th Al–Li Conference", Williamsburg, Virginia, 1989, edited by T. H. Sanders and E. A. Starke (MCE, 1989) pp. 837–848.
17. P. SAINFORT and P. GUYOT, in "3rd Al–Li Conference", Oxford, 1985, edited by C. Baker, P. J. Gregson, S. Harris and C. J. Peel (Institute of Metals, London, 1986) pp. 420–426.
18. Y. MIURA, K. YUSU, S. AIBE, M. FURUKAWA and M. NEMOTO, in "5th Al–Li Conference", Williamsburg, Virginia, 1989, edited by T. H. Sanders and E. A. Starke (MCE, 1989) pp. 827–836.
19. J. C. HUANG and A. J. ARDELL, in "4th Al–Li Conference", Paris, 1987, edited by G. Champier, B. Dubost, D. Miannay and L. Sabetay (Journal de Physique, 1987) pp. 373–383.
20. R. DE JESUS and A. J. ARDELL, in "5th Al–Li Conference" Williamsburg, Virginia, 1989, edited by T. H. Sanders and E. A. Starke (MCE, 1989) pp. 661–670.
21. S. J. HARRIS, B. NOBLE, K. DINSDALE and M. PRIDHAM, in "Aluminium Alloys: Their Physical and

Mechanical Properties" Conference, Charlottesville, Virginia, USA, 1986, edited by T. H. Sanders and E. A. Starke (AIME, 1987) Vol. 2, p. 755.
22. M. HAYASHI and H. OIKAWA, *J. Jpn Inst. Light Metals* **36** (1986) 768.
23. E. N. DA C. ANDRADE and B. CHALMERS, *Proc. Roy. Soc.* **138A** (1932) 348.
24. P. L. TETLOW, PhD thesis, Queen Mary and Westfield College, University of London (1991) p. 123.
25. A. G. OLDER, PhD thesis, Queen Mary and Westfield College, University of London (1986) p. 239.
26. P. M. KELLY, A. JOSTSONS, R. G. BLAKE and J. G. NAPIER, *Phys Status Solidi* **31a** (1975) 771.
27. C. K. L. DAVIES, P. NASH and R. N. STEVENS, *Acta Metall.* **28** (1980) 179.
28. M. FURUKAWA, Y. MIURA and N. NEMOTO, *Trans. Jpn Inst. Metals* **26** (1985) 225; also in "3rd Al–Li Conference", Oxford, 1985, edited by C. Baker, P. J. Gregson, S. J. Harris and C. J. Peel (Institute of Metals, London, 1986) pp. 427–434.
29. W. A. CASSADA, G. J. SHIFLET and E. A. STARKE, *Acta Metall.* **34** (1986) 367.
30. J. C. HUANG and A. J. ARDELL, *Mater. Sci. Engng* **A104** (1988) 149.
31. S. F. BAUMANN and D. B. WILLIAMS, in "2nd Al–Li Conference", Monterey, California, 1983, edited by T. H. Sanders and E. A. Starke (AIME, Warrendale, PA, 1984) pp. 17–29.
32. P. J. GREGSON and H. M. FLOWER, *J. Mater. Sci. Lett.* **3** (1984) 829.
33. J. M. SILCOCK, *J. Inst. Metals* **89** (1961) 203.
34. M. CARRARD and J. L. MARTIN, *Phil. Mag. A* **56** (1987) 391.
35. *Idem, ibid.* **58** (1988) 491.
36. D. P. POPE and S. S. EZZ, *Int. Met. Rev.* **29** (1984) 136.
37. P. A. FLINN, *Trans. Met. Soc. AIME* **218** (1960) 145.
38. S. TAKEUCHI and E. KURAMOTO, *Acta Metall.* **21** (1973) 415.
39. C. C. WAN, H. SMALLEN and R. V. CARTER, in "5th Al–Li Conference", Williamsburg, Virginia, 1989, edited by T. H. Sanders and E. A. Starke (MCE, 1989) pp. 1553–1562.
40. X. XIAOXIN and J. W. MARTIN, in "4th Al–Li Conference", Paris, 1987, edited by G. Champier, B. Dubost, D. Miannay and L. Sabetay (Journal de Physique, 1987) pp. 433–438.
41. D. KHIREDDINE, R. RAHOUADJ and M. CLAVEL, *Acta Metall.* **37** (1989) 191.
42. H. MUGHRABI, *Acta Metall.* **31** (1983) 1367.

Received 18 September
and accepted 27 November 1991